

ORIGINAL ARTICLE

Open Access



Response of ion velocities of daytime ionospheric wavenumber-4 to solar activity observed by ROCSAT-1 and DEMETER

Ching-Chung Cheng¹, Jann-Yenq Liu^{1,2,3}, Fu-Yuan Chang^{1,2}, Chi-Yen Lin^{1,2}, Loren C. Chang^{1,2} and Chi-Kuang Chao^{1,2,3*}

Abstract

The electron/ion density/temperature and ion velocities observed by the ROCSAT-1 and DEMETER satellites are used to examine the daytime wavenumber-4 (WN4) feature in the equatorial/low latitude ionosphere during various months and solar activity levels of 1999–2010. A moving median process has been employed to isolate WN4 features and calculate their amplitudes, while the upward ion drift is used to estimate electric fields. The ROCSAT-1 and DEMETER ion density, ion temperature, and ion velocity generally yield prominent WN4 features over the center of Pacific Ocean, the west side of South America, the center of the Atlantic Ocean, and Southern India. The correlation coefficient between the deviation of ion density and upward ion drift is significant during high solar activity of 1999–2004, while it approaches to zero during low solar activity of 2004–2010. This confirms that the longitudinal variation of the upward ion drift is essential during high solar activity, and the associated amplitude of dynamo eastward electric field is in the range of 0.10–0.14 mV/m, which is 15–19% of daily dynamo electric field. By contrast, the deviation of the ion density and the northward field-aligned ion flow show a clear anti-correlation which yields a maximum coefficient in August during low solar activity but no correlation during high solar activity. These indicate that the longitudinal variation of the meridional field-aligned ion flow could play an important role during low solar activity, and its amplitude is in the range of 10.44–13.91 m/s, which is 10–13% of the ambient ion flows.

Keywords Wavenumber-4, Solar activity, $E \times B$ drift, Meridional ion flow, Dynamo electric field, DEMETER, ROCSAT-1

1 Introduction

Wavenumber-four (WN4) structures in the ionosphere have been intensively studied using the nighttime OI 135.6-nm emission (Sagawa et al. 2005; Henderson et al. 2005; Immel et al. 2006), ionospheric total electron

content (TEC) (Lin et al. 2007), magnetometer observations of the equatorial electrojet (England et al. 2006), ion species in F-region (Bankov et al. 2009), and vertical ion drift velocity (Hartman and Heelis 2007; Kil et al. 2007; Fejer et al. 2008; Liu et al. 2023). Clear WN4 features can be observed over the center of Pacific Ocean (PO), the west side of South America (SA), the center of the Atlantic Ocean (AO), and Southern India (SI). There is strong evidence that the WN4 feature is associated with diurnal eastward wavenumber 3 (DE3) nonmigrating tides since the tidal winds contribute to the E-region electric fields which in turn map to the F-region and modulates vertical $E \times B$ plasma drifts that finally control the EIA structure. (Immel et al. 2006; Hagan et al. 2007; Wan et al. 2010).

*Correspondence:

Chi-Kuang Chao
chikuang.chao@g.ncu.edu.tw

¹ Department of Space Science and Engineering, National Central University, No. 300, Zhongda Rd., Zhongli District, Taoyuan City 320317, Taiwan

² Center for Astronautical Physics and Engineering, National Central University, Taoyuan City 320317, Taiwan

³ Center for Space and Remote Sensing Research, National Central University, Taoyuan City 320317, Taiwan



Lin et al. (2007) examined electron density profiles sounded by FORMOSAT-3/COSMIC (Constellation Observing System for Meteorology Ionosphere and Climate) in 2006 and found that the WN4 structure of TEC starts to develop at 0800–1000 local time (LT) and becomes the most prominent at 1200–1600 LT. Kil et al. (2008) and Fejer et al. (2008) studied ROCSAT-1 (Republic of China Satellite 1) data and reported that during 0900–1200 LT equinox and June solstice, WN4 peaks in vertical ion drift velocity appear collocated with longitudinal maximums in ion density. These studies show that WN4 becomes prominent during the daytime. Bankov et al. (2009) examined observations of DMSP (Defense Meteorological Satellite Program) and DEMETER (Detection of Electromagnetic Emissions Transmitted from Earthquake Regions) in 2004, and propose that longitude variations of WN4 structures driven by F-region winds are present at all local times in the topside ionosphere and modulate the magnitude and location of the peak WN4 variations during the daytime and the nighttime. Kakinami et al. (2011) analyzed observations of DEMETER from July to October 2007 and Hinotori from July to October 1981, and suggest that longitudinal structure of electron density in the topside ionosphere is produced not only by the modulated electric field by nonmigrating tides in the dynamo region but also by meridional wind effects at the satellite altitude. On the other hand, Wan et al. (2008) examine the WN4 intensity in TEC under 3 solar activity levels of $F10.7 < 120$, $120 < F10.7 < 160$, and $F10.7 > 160$ and find that the WN4 intensity in TEC is increased with solar flux. Oberheide et al. (2009) reported that solar cycle effects become more important above 120 km in the E region, where DE3 tidal winds modulate the electric fields. Onohara et al. (2018) analyzed FORMOSAT-3/COSMIC observations and found that the DE3 amplitude in $hmF2$ is the most prominent in high solar activity period of 2013, while that in $NmF2$ is pronounced during 2007, 2008, and 2015. These results indicate strong solar activity dependency in WN4 features. In this paper, to derive the dynamo electric field mapped from the E-region and to clarify the WN4 response of ion velocities to solar activity, we examine observations from the ROCSAT-1 and DEMETER satellites, and find the correlation between ion density and vertical/meridional ion velocities, and compute the associated dynamo electric fields over WN4 in various months and years.

2 Observation

ROCSAT-1 had a circular orbit at an average altitude of 600 km with an inclination of 35° (Chang et al. 1999; Su et al. 1999; Yeh et al. 1999). Its low-inclination orbit enabled ROCSAT-1 to sample the low latitude ionosphere

within $\pm 35^\circ$ geographic latitude during all local times approximately every 25 days. IPEI (Ionospheric Plasma and Electrodynamics Instrument) onboard ROCSAT-1 measures the ion density (N_i), ion temperature (T_i), as well as upward ion drift perpendicular to the magnetic field on the meridian plane (V_z) and northward field-aligned ion flow (V_y) during March 1999–June 2004. On the other hand, DEMETER traveled in a circular sun-synchronous orbit with the descending node at 1030LT and ascending node at 2230LT, an altitude of 660 km, and an inclination of 98° , with observations covering $\pm 65^\circ$ geomagnetic latitude every 15 days (Cussac et al. 2006). Onboard measurements of plasma quantities include ISL (Instrument Sonde de Langmuir) observations of the ion and electron density (N_i and N_e) and electron temperature (T_e), and IAP (Instrument d'Analyse du Plasma) measuring the ion temperature (T_i) and ion velocities (V_z and V_y) during July 2004–December 2010. For cross-comparisons, DEMETER ion velocities (V_z and V_y) have been converted to the magnetic coordinate. ROCSAT-1 plasma data in January and March 2001 are discarded owing to an insufficient number of available data points to construct constant LT maps. The accuracy of the ion drift meter onboard the satellite depends on the proportion of oxygen ions and light ions such as hydrogen ions since oxygen ions produce a sharper spot than hydrogen ions on the collector on IAP, which improves the accuracy of the velocity direction measurement (Berthelier et al. 2006). Thus, ion velocities probed by the ion drift meter with the percentage of hydrogen ions above 15% have been removed in the following study. The ROCSAT-1 and DEMETER data allow us to examine the WN4 response to the high solar activity years of 1999–2004 (average $F10.7 = 160.5$ sfu) and low solar activity years of 2004–2010 (average $F10.7 = 82.4$ sfu), respectively. Their upward ion velocity measurements are further used to estimate the dynamo electric fields.

We focus on quiet time ($K_p \leq 3$) observations of ROCSAT-1 during 0900–1200 LT and DEMETER at 1030 LT in the equatorial/low latitude ionosphere within $\pm 30^\circ$ dip latitude. The ion density, ion temperature, and ion velocity probed by the two satellites, are smoothed by a moving window of 20° in latitude by 20° in longitude, sliding by 2° in latitude and 10° in longitude, to obtain mean values without high-frequency and unwanted noises. Figure 1 displays prominent WN4 features in ROCSAT-1 N_i , T_i , and V_z as well as in DEMETER N_i , N_e , T_i , T_e , V_z , and V_y within $\pm 15^\circ$ dip latitude. However, no clear features in ROCSAT-1 V_y can be observed around the dip equator. Similar patterns of N_e versus N_i and T_e versus T_i probed by DEMETER reveal the characteristics of quasi-neutrality and thermal equilibrium. Following Bankov et al. (2009), to further recognize the WN4 signature, large

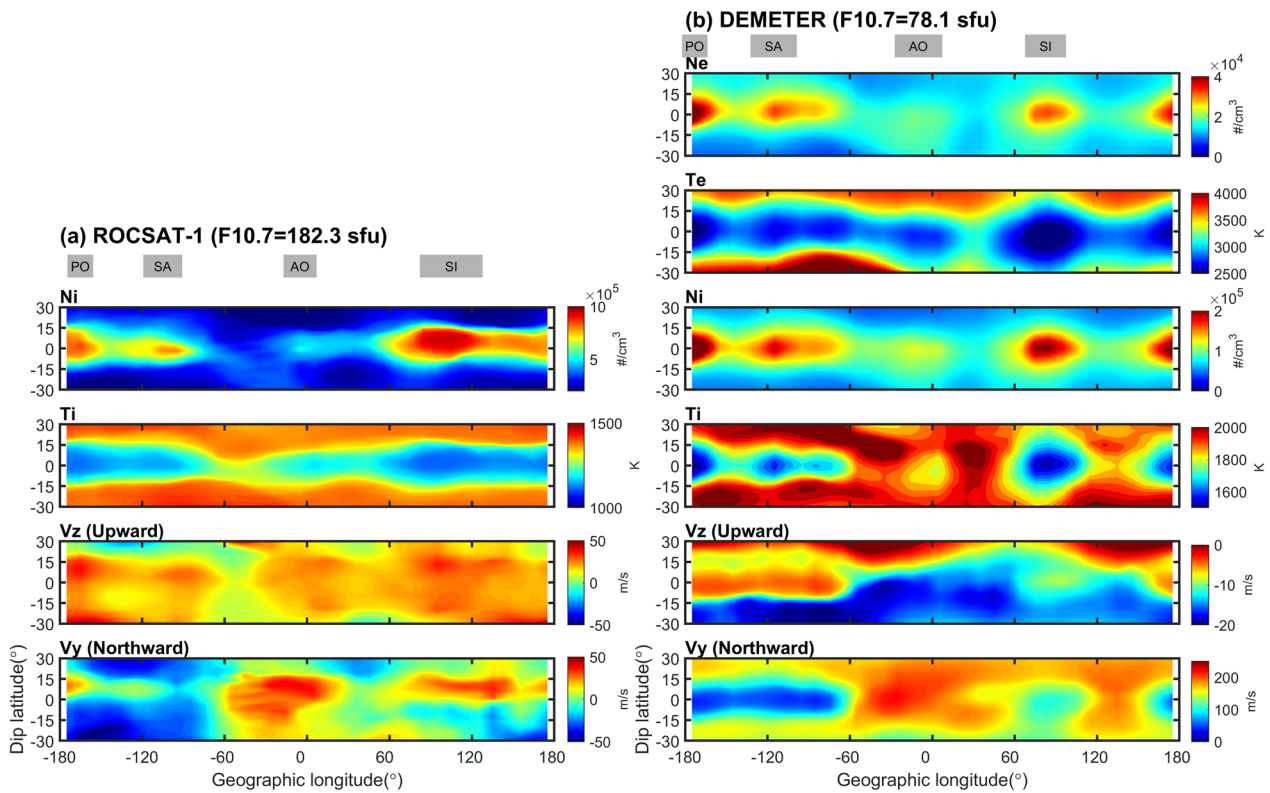


Fig. 1 Constant LT maps of plasma quantities probed by **a** ROCSAT-1 in 0900–1200LT in September 2000 and those by **b** DEMETER at 1030LT in September 2006. The spatial resolutions are 2° in dip latitude and 10° in geographic longitude. The monthly median of F10.7 in September 2000 and 2006 is denoted in the figure

scale variations are removed by applying the deviation data $\delta A = \text{smooth}(A) - \text{median}(A)$, where $\text{smooth}(A)$ is the smoothed constant LT map (Fig. 1), and $\text{median}(A)$ is 90° (i.e. $\pm 45^\circ$) longitudinal running median. Figure 2 illustrates pronounced WN4 signatures in ROCSAT-1 δN_i , δT_i , and δV_z and those in DEMETER δN_i , δN_e , δT_i , δT_e , δV_z and δV_y within $\pm 15^\circ$ dip latitudes. It can be found that the weakest signature over the AO in Fig. 1 has been remarkably enhanced in Fig. 2. Similar to Fig. 1, no obvious features in ROCSAT-1 δV_y can be observed. By contrast, over the WN4 longitudes, DEMETER δV_z is positive, while the associated δV_y is mainly negative except for AO. In general, DEMETER WN4 signatures can be found around the dip equator over PO, SA, and SI, while a weak one over AO tends to move toward south side of the dip equator.

Figure 3 illustrates that the monthly variation of all plasma quantities within $\pm 15^\circ$ dip latitude yield very similar WN4 patterns during 1999–2010. Due to the Coulomb cooling process, δT_i tends to have an opposite polarity to δN_i . The WN4 signatures of δN_i and δT_i over the PO simultaneously shift 10–20 longitudes toward west in January–June and backward east in July–December, while those over SA shift 10–20 longitudes

toward east in January–June and backward west in July–December, which reveals a C-shape and an inverted C-shape features, respectively. It should be noticed that ROCSAT-1 δV_z and DEMETER δV_y also yield the same behavior. Figure 3a displays that for ROCSAT-1, δN_i , δT_i , and δV_z exhibit very prominent WN4 features mainly in March equinox months (i.e., February–April) and September–November during 1999–2004. Note that no similar features can be found in δV_y . By contrast, for DEMETER, Fig. 3b depicts that WN4 signatures in δV_z can be identified from September to December, and however three troughs in δV_y over the PO, SA, and SI are clearly observed during 2004–2010.

Figure 4, extracting data used in Fig. 3, illustrates the correlation of δN_i vs δV_z and δN_i vs δV_y observed by ROCSAT-1 (i.e., high solar activity), and those by DEMETER (i.e., low solar activity). For the high solar activity period, the correlation coefficient of δN_i vs δV_z , $R(\delta N_i \text{ vs } \delta V_z) = 0.64$ (0.62, 0.67), shows that WN4 signatures are significantly related to the deviation of the upward ion drift (Fig. 4a). Here, the numbers in the parentheses stand for the associated 95% confidence interval for the correlation coefficient. When the 95% confidence interval includes 0, the data do not provide significant evidence at

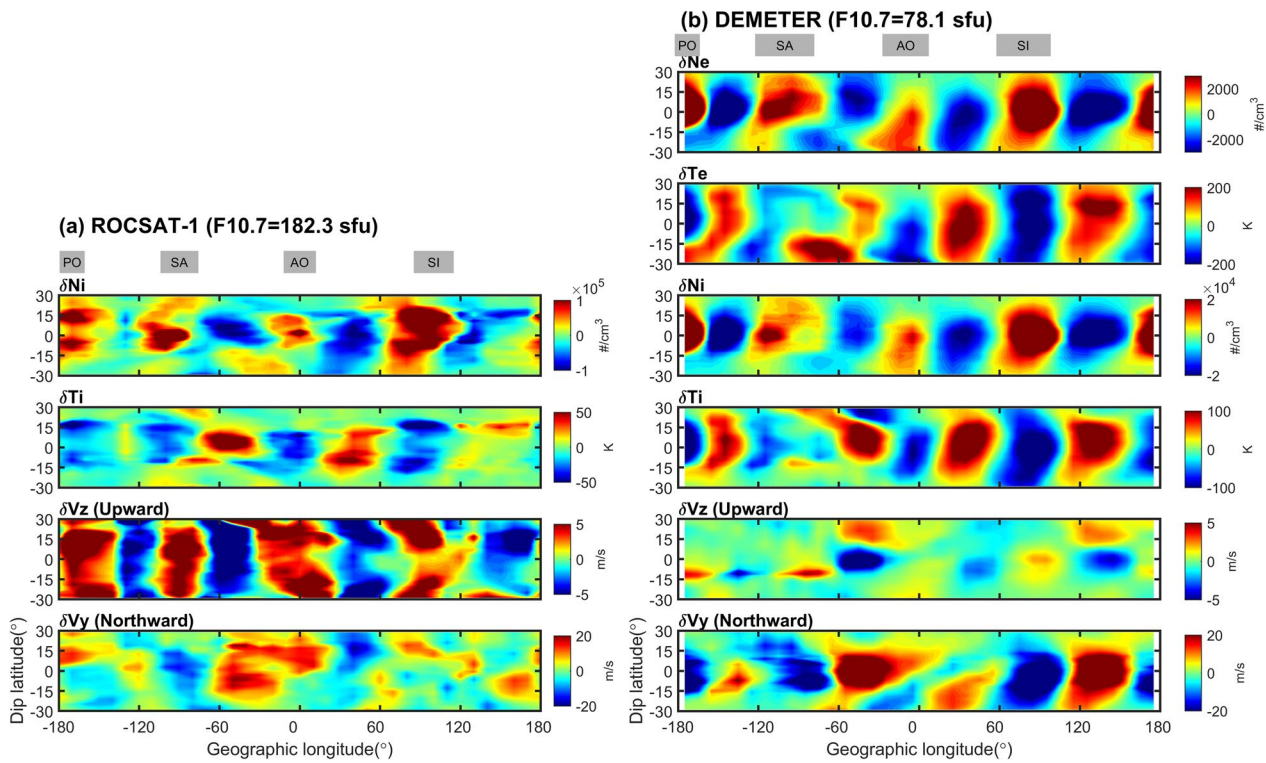


Fig. 2 Deviation LT maps of the plasma quantities of **a** ROCSAT-1 in 0900–1200LT in September 2000 and those by **b** DEMETER at 1030LT in September 2006. The spatial resolutions are the same as Fig. 1

level 0.05 for different proportions (i.e., the proportion-difference is not significant) (Klotz and Johnson 1983). By contrast, $R(\delta N_i \text{ vs } \delta V_y) = 0.11$ (0.06, 0.15) suggests the correlation being rather weak. Nevertheless, these results show that the longitudinal variation of the upward ion drift is the dominant WN4 formation mechanism during the high solar activity. For the low solar activity period, on the other hand, $R(\delta N_i \text{ vs } \delta V_z) = -0.02$ (-0.06, 0.01) indicates that the deviation of the upward ion drift is insignificant to the WN4 features. In contrast, anti-correlation of $R(\delta N_i \text{ vs } \delta V_y) = -0.45$ (-0.48, -0.41) suggests that the deviation of the meridional ion flows better correlates with WN4 features in the deviation of the ion density.

Table 1 lists the WN4 amplitudes of the deviation of the ion density, ion temperature, and ion velocities at the four longitudes during the high and low solar activities. The overall amplitude is calculated by the average of amplitudes over the four WN4 longitude regions. The overall amplitudes of δN_i and δT_i during the high (low) solar activity are 0.58 (0.13) $\times 10^5$ \#/cm^3 and 22.73 (62.35) K, which reveals that δN_i is larger in the high solar activity, while δT_i is oppositely greater in the low solar activity. Based on $R(\delta N_i \text{ vs } \delta V_z)$ of ROCSAT-1 and $R(\delta N_i \text{ vs } \delta V_y)$ of DEMETER being significant (Fig. 4), we calculate the

WN4 amplitudes of ROCSAT-1 δV_z , and those of DEMETER δV_y . Amplitudes of δV_z range from 3.67 – 3.90 m/s with an average of 3.79 m/s. According to Kelley (2009) and magnetic fields from International Geomagnetic Reference Field, amplitudes of the associated eastward dynamo electric fields ranging from 0.10 – 0.14 mV/m with an overall average of 0.11 mV/m are derived by δV_z . On the other hand, amplitudes of δV_y range from 10.44 – 13.91 m/s with an average of 12.06 m/s during the low solar activity. To remove the ambient effect, the normalized WN4 amplitude $\overline{\delta A} (= \frac{\text{amp}(\delta A)}{\text{median}(\delta A)})$, where A is the plasma quantities, $\text{amp}(\delta A)$ is the amplitude of deviation plasma quantities over four WN4 regions, and $\text{median}(\delta A)$ is the median value of the deviation plasma quantity in overall longitudes. Table 2 displays that $\overline{\delta N_i}$ ($\overline{\delta T_i}$) at the four WN4 regions are either equal or larger in the high (low) solar activity, except $\overline{\delta N_i}$ at PO. Table 1 depicts that the amplitude of δN_i is larger in the high solar activity and δT_i is greater in the low solar activity, while Table 2 reveals that ROCSAT-1 $\overline{\delta T_i}$ is larger in low solar activity. Results from Tables 1 and 2 confirm that the influence of solar activity on δN_i and δT_i are significant, and however that on $\overline{\delta N_i}$ and $\overline{\delta T_i}$ are insignificant.

We further examine monthly variations of $R(\delta N_i \text{ vs } \delta V_z)$ and $R(\delta N_i \text{ vs } \delta V_y)$ during the two solar activities.

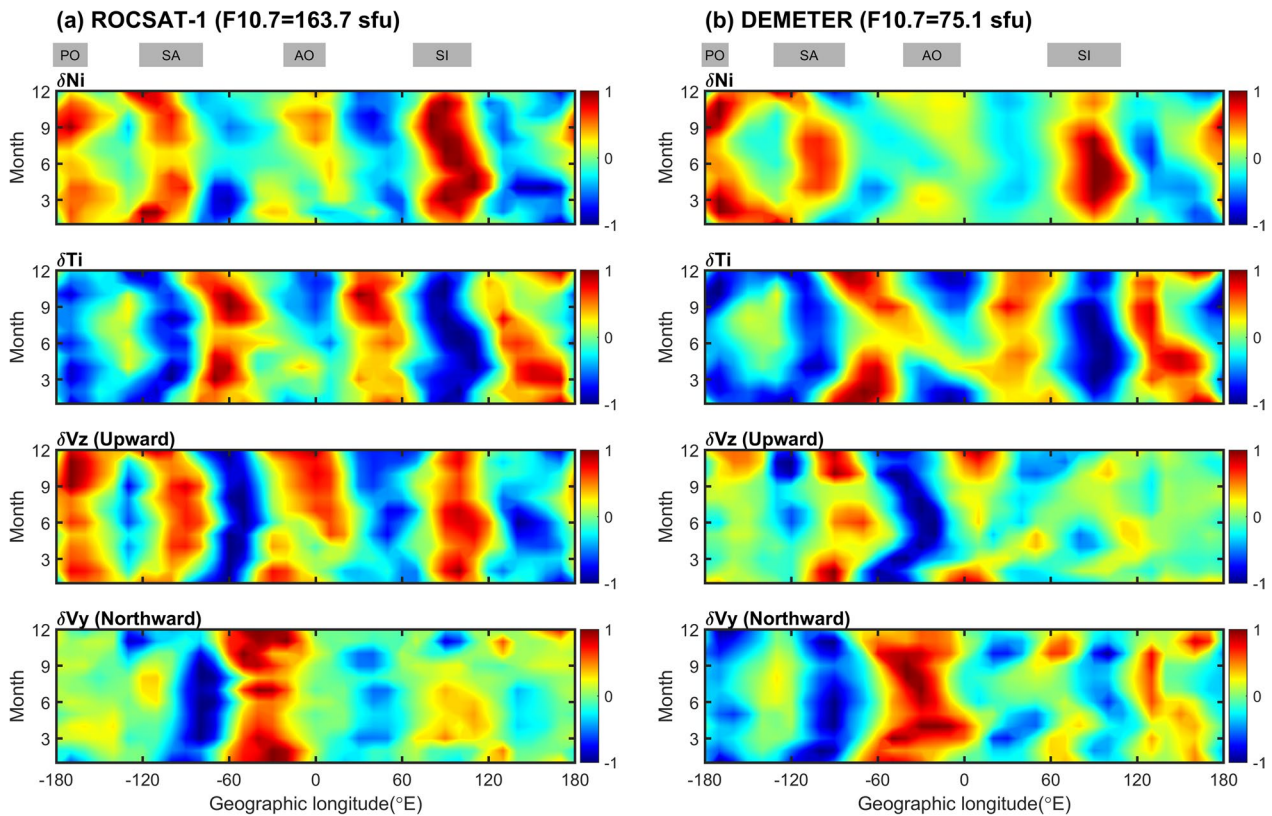


Fig. 3 Monthly variations in WN4 signatures of the normalized plasma quantities within $\pm 15^\circ$ dip latitudes observed by ROCSAT-1 during **a** July 1999–May 2004 and DEMETER during **b** July 2004–December 2010. The plasma quantities in each longitude are divided by their associated longitudinal maximum, and therefore the quantities are unitless

Figure 5a shows that $R(\delta N_i \text{ vs } \delta V_z)$ are all positive in various months, and yield a maximum value, 0.73, in August of the high solar activity years, while $R(\delta N_i \text{ vs } \delta V_y)$ are positive in March–September with a maximum in June, but negative in November–February with a minimum in December. Figure 5b illustrates that the coefficients $R(\delta N_i \text{ vs } \delta V_z)$ fluctuate around zero, while $R(\delta N_i \text{ vs } \delta V_y)$ are negative in all months with a maximum, 0.62, in August during low solar activity. Results in Fig. 5 show that the deviation of $E \times B$ drift is essential to the WN4 feature in various months during high solar activity, while the deviation of meridional field-aligned ion flows is significantly anti-correlated to that of ion densities, especially in June–September, in the low solar activity period.

3 Discussion and conclusion

Previous studies (Lin et al. 2007; Kil et al. 2007; Kakinami et al. 2011) reported clear WN4 features in the electron density, electron temperature, ion density, upward $E \times B$ drift, etc., which agree with those observed by ROCSAT-1 and DEMETER (Fig. 1). However, strong WN4 signatures in V_y and δV_y as well as insignificant signatures in V_z and δV_z in Figs. 1b and 2b evidently show

that the meridional ion flows are rather prominent than upward $E \times B$ drifts over WN4 regions during the low solar activity. A comparison between Figs. 1 and 2 suggests that the deviation data process proposed by Bankov et al. (2009) is useful to isolate the amplitude of WN4 signatures. Figures 1 and 2 show a clear anti-phase relationship between N_i and T_i (δN_i and δT_i) due to the Coulomb cooling process. Here, WN4 signatures in the ion temperature might be for the first time reported. Bankov et al. (2009) found that the WN4 signature in DEMETER N_i and δN_i over AO, where the declination is negative, is located southward of the magnetic equator, which can be explained by the combined effects of $E \times B$ drifts and meridional neutral winds. Figures 1b and 2b show that the WN4 signatures in N_i and δN_i over AO is shifted toward south side of the dip equator, which agrees with Bankov et al. (2009). Meanwhile, Figs. 1b and 2b also show prominent WN4 in V_y and δV_y , which once again agrees with Bankov et al. (2009) that the WN4 in the ion density is related to meridional neutral winds in low solar activity periods. Figure 3 illustrates that WN4 features in δN_i , δT_i , and δV_z become pronounced in March and September–November during high solar activity years

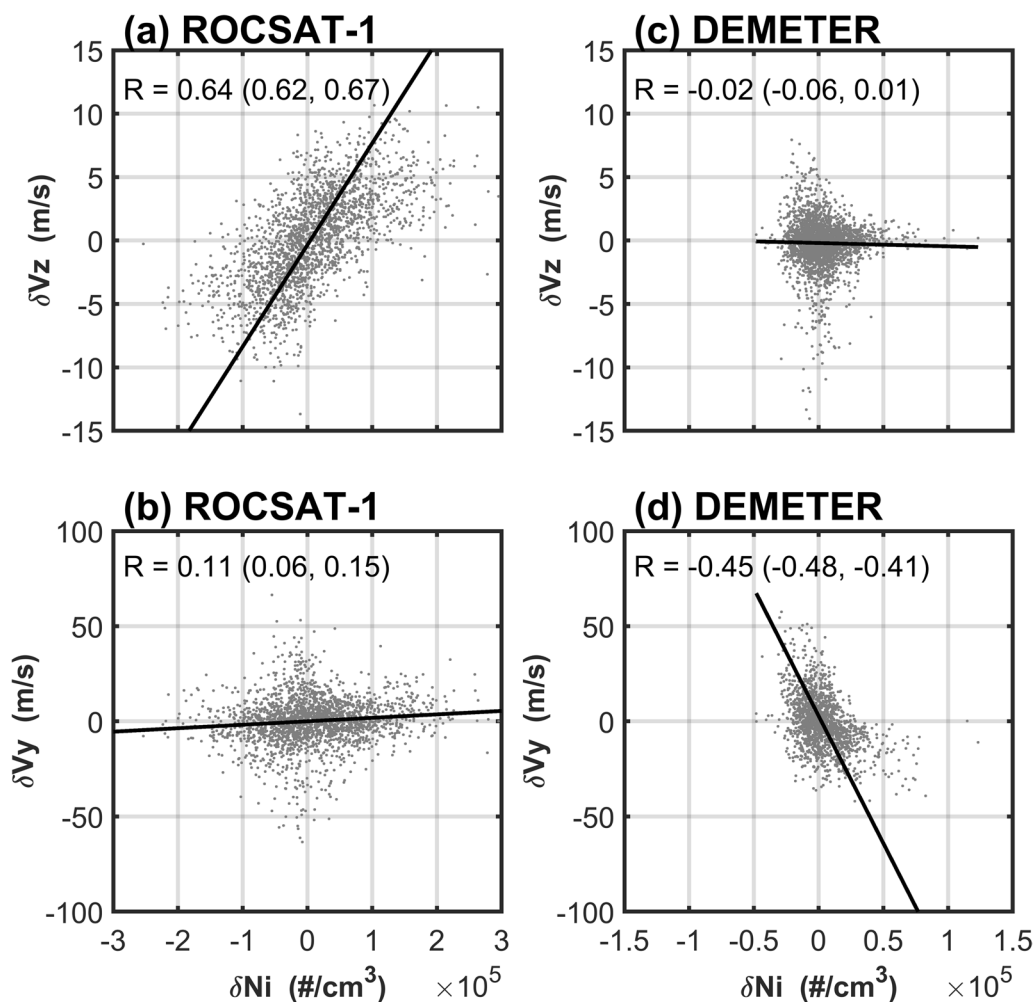


Fig. 4 Scatterplots of δN_i vs δV_z and δN_i vs δV_y observed by **a, b** ROCSAT-1 and **c, d** DEMETER. The black lines are the linear regression lines. The numbers in the parentheses stand for the associated 95% confidence interval for the correlation coefficient

Table 1 Amplitudes of WN4 Observed by ROCSAT-1 and DEMETER

ROCSAT-1	PO	SA	AO	SI	Overall
$\delta N_i (\times 10^5 \text{ \#/cm}^3)$	0.50	0.43	0.48	0.85	0.58
δT_i (K)	17.68	20.45	21.05	31.73	22.73
δV_z (m/s)	3.70	3.88	3.67	3.90	3.79
DEMETER					
$\delta N_i (\times 10^5 \text{ \#/cm}^3)$	0.15	0.10	0.07	0.18	0.13
δT_i (K)	51.92	54.34	50.45	80.63	62.35
δV_y (m/s)	10.44	13.91	11.85	12.05	12.06

Table 2 Normalized Amplitudes of WN4 Observed by ROCSAT-1 and DEMETER

ROCSAT-1	PO	SA	AO	SI	Overall
$\overline{\delta N_i}$	0.10	0.09	0.10	0.18	0.12
$\overline{\delta T_i}$	0.01	0.02	0.02	0.02	0.02
$\overline{\delta V_z}$	0.15	0.15	0.15	0.16	0.15
DEMETER					
$\overline{\delta N_i}$	0.14	0.09	0.07	0.17	0.12
$\overline{\delta T_i}$	0.03	0.03	0.03	0.05	0.03
$\overline{\delta V_y}$	0.07	0.10	0.08	0.08	0.08

of 1999–2004. The good agreement between the previous and current studies confirms that plasma quantities of the electron/ion density, electron/ion temperature, and ion velocity can be used to examine WN4 signatures.

Hartman and Heelis (2007) found that there is a seasonal variation of DMSP vertical $E \times B$ drifts (i.e. V_z) associated with WN4 shifting east during northern summer and west during northern winter, which generally agrees well

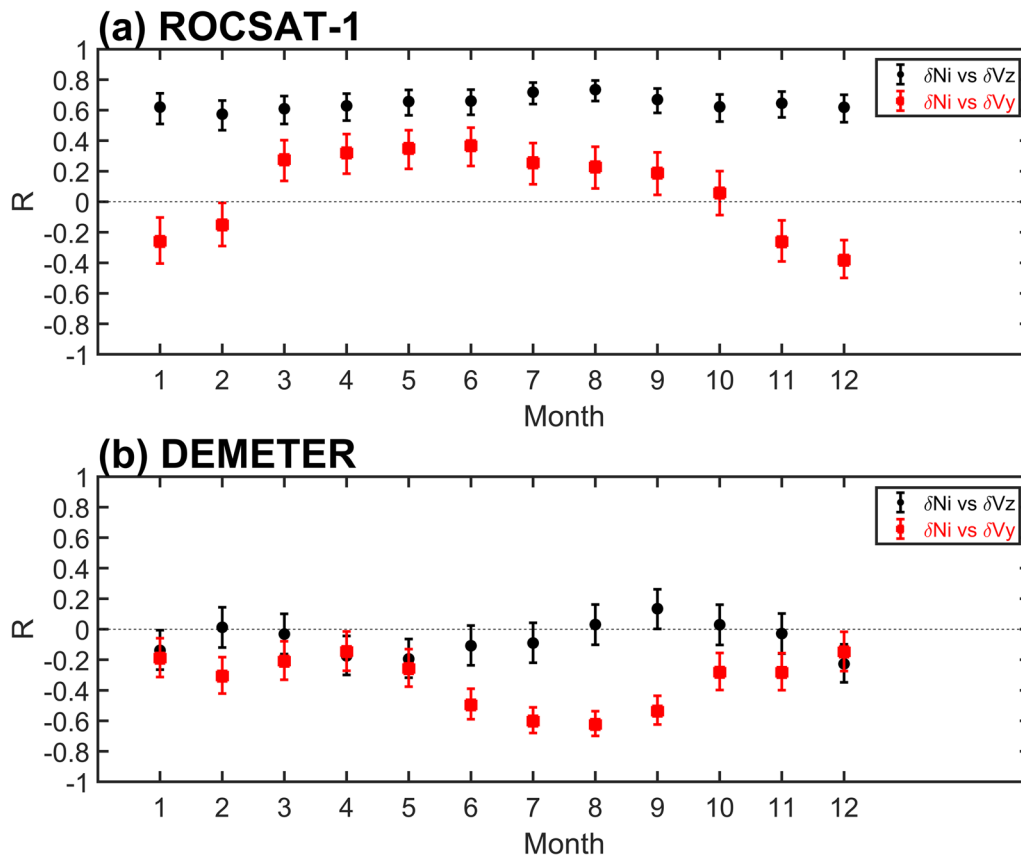


Fig. 5 $R(\delta N_i \text{ vs } \delta V_z)$ and $R(\delta N_i \text{ vs } \delta V_y)$ in various months and solar activities. Error bars are the upper and lower bounds for a 95% confidence interval for each coefficient

with Fig. 3 that WN4 in ROCSAT-1 δN_i , δT_i , and δV_z , as well as DEMETER δN_i , δT_i , and δV_y over SA (negative declination) displays the prominent inverse C-shape longitudinal motion toward the east in January–June and backward the west in July–December. Figure 3 also shows the C-shape longitudinal motion of WN4 in the above-mentioned parameters over PO (positive declination), which confirms the meridional wind effect being significant on different orientations of the magnetic meridian. The similar C-shape behavior in ROCSAT-1 δN_i , δT_i , and δV_z , as well as DEMETER δN_i , δT_i , and δV_y strongly indicates the relationship between the deviation of vertical $E \times B$ drift (meridional ion flow) and WN4 features in δN_i and δT_i in the high (low) solar activity.

The correlation of $R(\delta N_i \text{ vs } \delta V_z) = 0.64$ (0.62, 0.67) during 0900–1200LT in Fig. 4a shows that the upward $E \times B$ drift can significantly contribute to the WN4 formation in the morning period, which agrees with those reported by Kil et al. (2008) and Fejer et al. (2008). Meanwhile, Bankov et al. (2009) and Kakinami et al. (2011) suggest that the WN4 longitudinal structure might be also related to meridional winds. Additionally, Chang et al. (2020)

and Liu et al. (2023) report that summer-to-winter winds (or meridional field-aligned flows) significantly modify the longitudinal distribution of electron and ion density at the magnetic equator during low solar activity periods. Nonlinear wave interactions of the tides responsible to meridional winds, the offset of the magnetic equator, and the DE3 nonmigrating tide will give modifications of the WN4 structure in the electron density in different tidal modes (*cf.* England et al. 2010; Chang et al. 2013). During the low solar activity, the correlation of $R(\delta N_i \text{ vs } \delta V_z) = -0.02$ (−0.06, 0.01) indicates that the deviation of upward $E \times B$ drifts at the dip equator are insignificant (Figs. 4c), and however, $R(\delta N_i \text{ vs } \delta V_y) = -0.45$ (−0.48, −0.41) shows that the deviation of southward meridional ion flows to the WN4 ion density features plays an important role (Fig. 4d). This indicates that the deviation of the meridional ion flows becomes more related to the WN4 feature in the low solar activity. The correlation results in Fig. 4 well agree with the solar activity dependence of WN4 features seen in Figs. 1, 2, 3.

Tables 1 and 2 list the WN4 amplitudes and the normalized ones of the plasma quantities in various

longitude regions and solar activity levels. The amplitudes of δN_i are proportional to solar activities, which agrees with Wan et al. (2008) and Onohara et al. (2018). On the other hand, the amplitudes and normalized ones of δT_i , which might be for the first time reported, are found to be inversely proportional to solar activity. These show that the ion density and ion temperature are better to study WN4 features during high and low solar activities, respectively. Moreover, the amplitudes of δV_z seem consistent with variations in the vertical drift reported by the previous studies (Hartman and Heelis 2007; Kil et al. 2007; Fejer et al. 2008) during high solar activity periods. This agreement confirms that the vertical drift is essential to the WN4 signature during high solar activities. The amplitudes of the associated dynamo electric fields are also derived. Based on Cheng et al. (2022) that derive the daily dynamo electric fields using the vertical $E \times B$ drifts, the amplitudes of the electric fields over the WN4 regions are 15–19% to the daily dynamo electric fields. On the other hand, the significant correlation of $R(\delta N_i \text{ vs } \delta V_y) = -0.45$ ($-0.48, -0.41$) allows us calculating amplitudes of δV_y . Table 1 depicts that the amplitude of δV_y lies between 10.44 and 13.91 m/s, which is about 10–13% to the associated ambient ion flows. These indicate that the meridional ion flow plays an important role to modulate the WN4 feature during low solar activities, and the amplitude of the deviation of ion flows is for the first time reported.

Scientists (Kil et al. 2008; Fejer et al. 2008) find that daytime upward drifts have strong WN4 signatures during equinox and June solstice, which agrees well with Fig. 5a that correlation coefficients of the deviation of the upward $E \times B$ drift versus that of the ion density are significant in all months and yield the prominent ones in June–September during the high solar activity period. On the contrary, Fig. 5b exhibits that correlation coefficients of the deviation of the upward $E \times B$ drift are mostly insignificant, and however, correlation coefficients of the deviation of the southward ion flow become pronounced in all seasons of low solar activity periods. Note that the tendency of monthly variations of $R(\delta N_i, \delta V_z)$ and $R(\delta N_i, \delta V_y)$ are similar exhibiting minimums during June–September, which generally agrees with June–October reported by previous scientists (Forbes et al. 2008; Kil et al. 2008; Pedatella et al. 2008; Ren et al. 2008; Liu et al. 2009; Häusler and Lühr 2009). In addition, Fig. 5b shows that the deviation of southward flows becomes more correlated to that of ion densities rather than upward $E \times B$ drifts, especially in August during low solar activity periods. Nonetheless, the negative $R(\delta N_i, \delta V_y)$ in various seasons shown in Fig. 5b well agrees with Fig. 4d, which confirms that the deviation of southward ion flows has a strong relationship with that of the ion density over the

WN4 regions during low solar activity. To explore the response of WN4 to various solar activities in detail, we further subgroup the ROCSAT-1 and DEMETER dataset into 4 solar activity levels from high to low: $F10.7 > 170$ (SA1), $130 < F10.7 < 170$ (SA2), $80 < F10.7 < 130$ (SA3), and $F10.7 < 80$ (SA4). Figure 6 illustrates that $R(\delta N_i \text{ vs } \delta V_z)$ in SA1, SA2, and SA3 are 0.69, 0.62, and 0.39, respectively, which shows that δN_i is proportional to δV_z . This agrees with that the WN4 intensity in TEC is increased with solar flux reached by Wan et al. (2008). Notice that $R(\delta N_i \text{ vs } \delta V_z)$ of -0.04 in SA4 is insignificant due to the 95% confidence interval including 0. These indicate that the deviation of the vertical ion drift to the WN4 peaks of δN_i plays an important role during the high solar activity. Figure 7 depicts that $R(\delta N_i \text{ vs } \delta V_y)$ yield small values of 0.16, 0.03, and -0.05 during SA1, SA2, and SA3. Note that the latter two include 0, and therefore, these three correlations are generally insignificant. By contrast, $R(\delta N_i \text{ vs } \delta V_y)$ of -0.44 in SA4 shows that the deviation of the southward ion flow is related to that of the ion density during the low solar activity.

Since DEMETER flew at sun-synchronized orbit of 98 degrees and ROCSAT-1 flew at 35 degrees inclination, there might be effects of the orbit inclinations embedded in the ion velocity data. Thus, ion parameters measured by ICON/IVM, flying at a satellite inclination of 27 degrees and in low solar activity years of 2019–2022, are used to cross-compare with our results. Figure 8 depicts prominent WN4 features in ICON V_y , which agrees with Fig. 1b except for AO. In addition, N_i , T_i , and V_z for ROCSAT-1 (Fig. 1a), DEMETER (Fig. 1b), and ICON (Fig. 8) exhibit similar longitudinal pattern at various solar activity levels and satellite inclinations. These similarities show that the WN4 longitudinal pattern in the ion parameters can be clearly detected regardless satellite inclinations.

Majority of the previous studies suggest the same that low solar activity prompts clearer WN4 or DE3 patterns. However, Wan et al. (2008) reveal that WN4 intensity in TEC is stronger during high solar activity, while Wan et al. (2010) find that the MLT parameters of TEC and neutral winds in DE3 are stronger during low solar activity. TEC is the integration of electron density along the altitude. As a result, TEC and its WN4 intensity should be dependent on $hmF2$ and $NmF2$. Note that Onohara et al. (2018) find that WN4 in $hmF2$, which is mainly modulated by the vertical $E \times B$ drift, is stronger in high solar activity, while WN4 in $NmF2$ is stronger in the low solar activity. In the meantime, Figs. 1, 2, 3 illustrate that V_z and δV_z (V_y and δV_y) exhibit prominent WN4 signatures and Figs. 4, 5, 6 depict that the correlation coefficient of δN_i and δV_z (δN_i and δV_y) is more significant in the high (low) solar activity. Our results and previous studies of

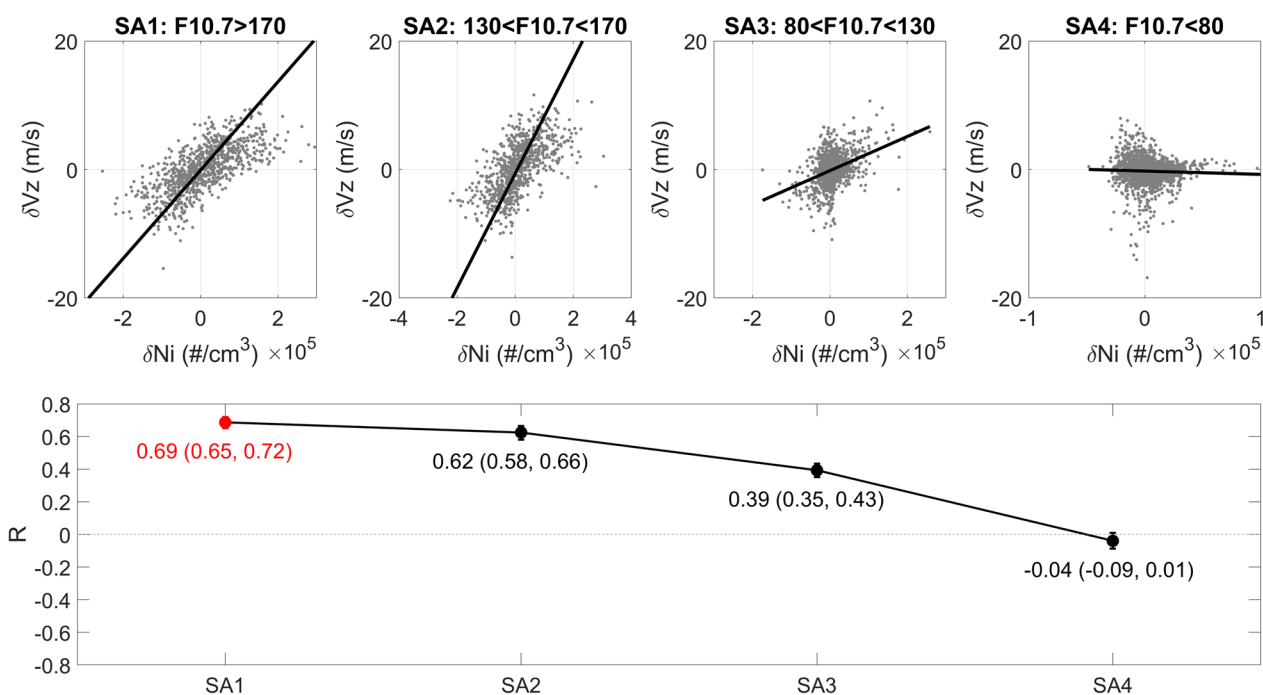


Fig. 6 Solar activity variation of $R(\delta Ni$ vs $\delta V_z)$. The red dot in the lower panel denotes the largest absolute value of R . Black solid lines in upper panels are linear regression lines. Error bars in the lower panel stand for the upper and lower bounds for a 95% confidence interval for each coefficient

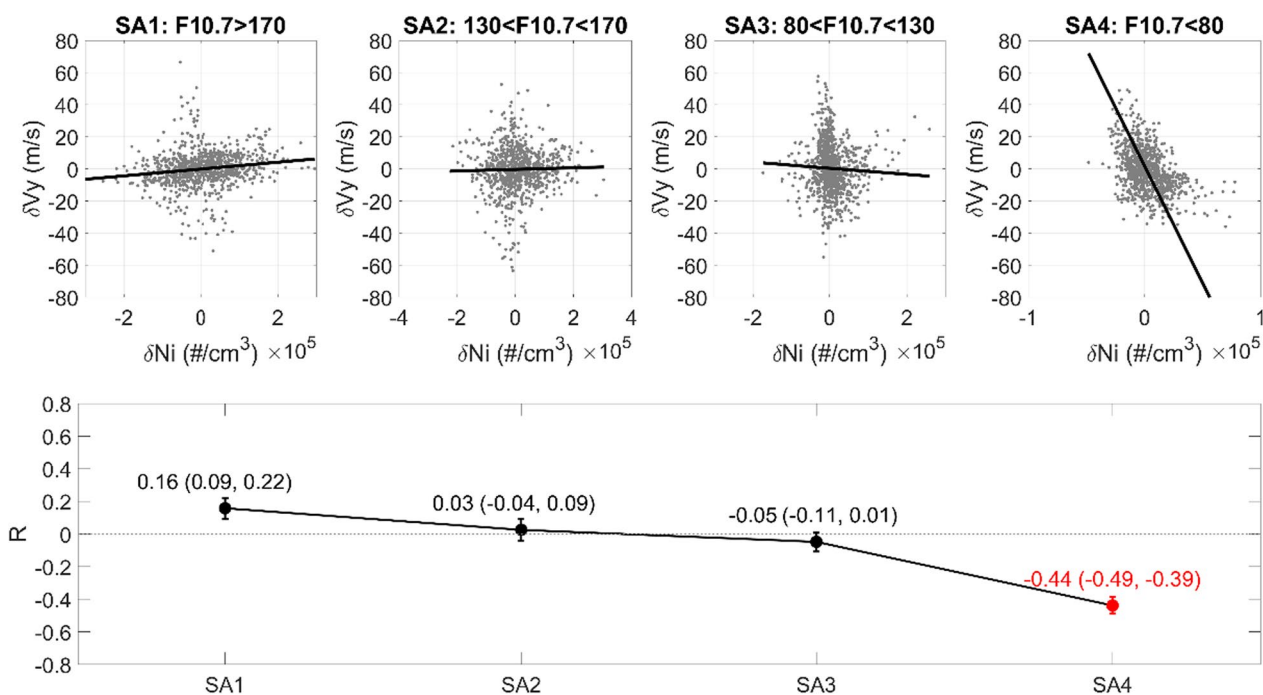


Fig. 7 Similar to Fig. 6 but for $R(\delta Ni$ vs $\delta V_y)$. The red dot in the lower panel denotes the largest absolute value of R

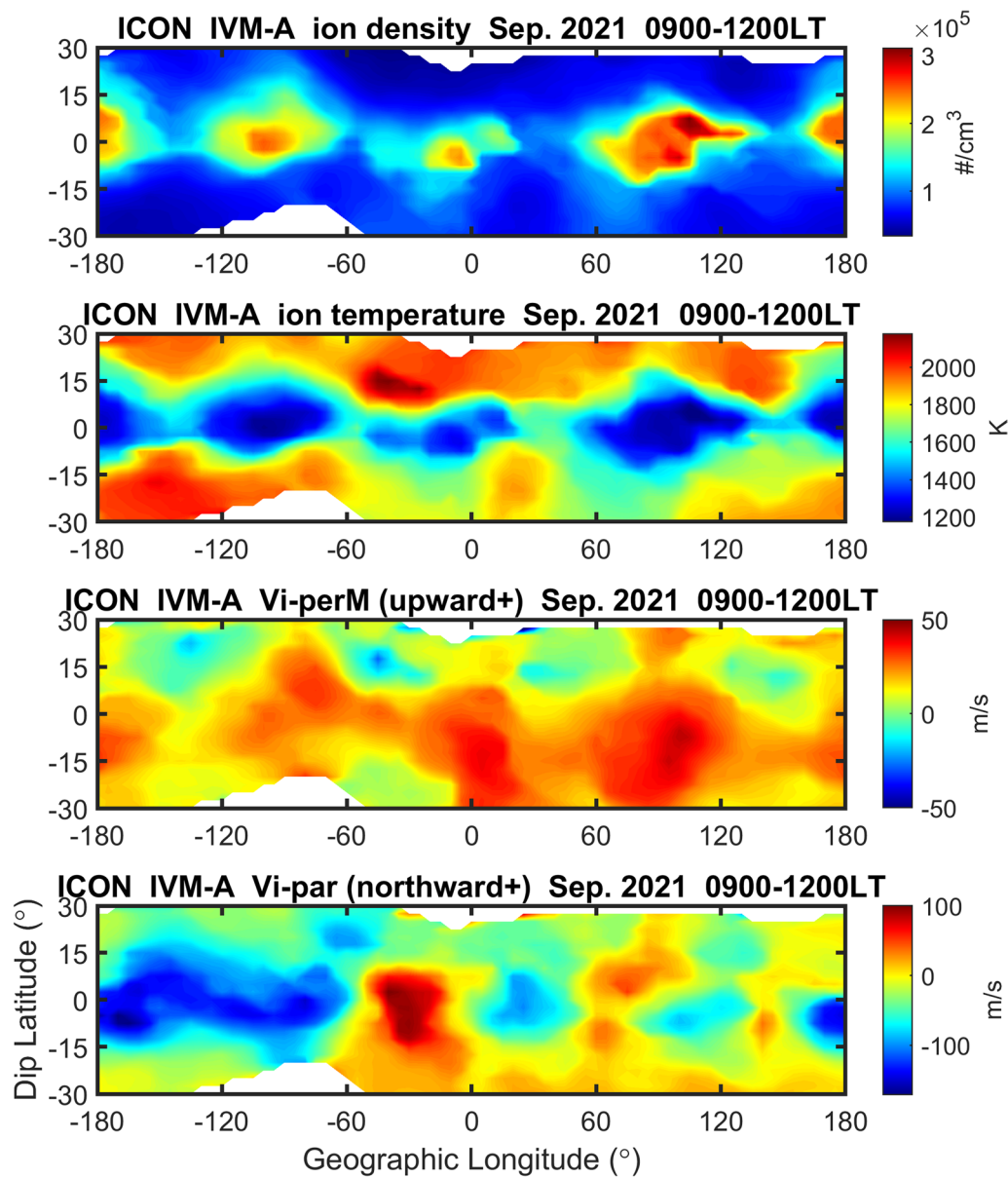


Fig. 8 Constant LT maps of plasma quantities probed by ICON IVM-A in 0900-1200LT in September 2021. The spatial resolution is the same as Fig. 1. The monthly median of F10.7 is 88.4 sfu

Wan et al. (2008), Wan et al. (2010), and Onohara et al. (2018) show that WN4 signatures in $hmF2$, $NmF2$, TEC, neutral winds, and ion velocities are a function of the solar activity. In conclusion, upward $E \times B$ drifts modulated by the dynamo electric fields is the major driver in forming WN4 features during high solar activity, and meridional winds can heavily modify the WN4 feature in the low solar activity.

Acknowledgements

This work was financially supported by the Center for Astronautical Physics and Engineering (CAPE) from the Featured Area Research Center program within the Higher Education Sprout Project by the Ministry of Education (MOE)

in Taiwan. This study is supported by the National Science and Technology Council (NSTC) Grant NSTC 112-2123-M-008-003 and MOST 111-2111-M-008-018 and MOST 111-2111-M-008-031 in Taiwan.

Author contributions

All the authors have equal contributions, read the manuscript, and agree to publish this paper.

Data availability

The ROCSAT-1 data is retrieved from NASA's Coordinated Data Analysis Web (CDAWEB) (<https://cdaweb.gsfc.nasa.gov/index.html/>), the DEMETER data is obtained from Centre de données de la Physique des Plasmas (CDPP) (<https://cdpp-archive.cnes.fr/>), and solar index F10.7 is got from the Space Physics Data Facility (SPDF) (<https://omniweb.gsfc.nasa.gov/form/dx1.html>).

Declarations

Competing interests

This paper has no competing and/or conflict interests with any other persons or organizations.

Received: 9 July 2023 Accepted: 10 April 2024

Published online: 10 May 2024

References

- Bankov L, Heelis R, Parrot M, Berthelier J-J, Marinov P, Vassileva A (2009) WN4 effect on longitudinal distribution of different ion species in the topside ionosphere at low latitudes by means of DEMETER, DMSP-F13 and DMSP-F15 data. *Ann Geophys* 27:2893–2902. <https://doi.org/10.5194/angeo-27-2893-2009>
- Berthelier JJ, Godefroya M, Leblanca F, Serana E, Pescharada D, Gilberta P, Artrub J (2006) IAP, the thermal plasma analyzer on DEMETER. *Planet Space Sci*. <https://doi.org/10.1016/j.pss.2005.10.018>
- Chang Y-S, Chiang W-L, Ying S-Y, Holt BJ, Lippincott CR, Hsieh K-C (1999) System architecture of the IPEI payload on ROCSAT-1. *Terrestrial Atmos Oceanic Sci* 10:7–18
- Chang LC, Lin CH, Yue J, Liu JY, Lin JT (2013) Stationary planetary wave and nonmigrating tidal signatures in ionospheric wave 3 and wave 4 variations in 2007–2011 FORMOSAT-3/COSMIC observations. *J Geophys Res Space Phys* 118:6651–6665. <https://doi.org/10.1002/jgra.50583>
- Chang FY, Liu JY, Fang TW, Rajesh PK, Lin CH (2020) Plasma depletion bays in the equatorial ionosphere observed by FORMOSAT-3/COSMIC during 2007–2014. *J Geophys Res Space Phys* 125:e2019JA027501. <https://doi.org/10.1029/2019JA027501>
- Cheng C-C, Liu J-Y, Lin CCH, Cheng Y-C (2022) Daily dynamo electric fields derived by using equatorial ionization anomaly crests of the total electron content. *Space Weather* 20:e2022SW003073. <https://doi.org/10.1029/2022SW003073>
- Cussac T, Clair M, Ulte-Guerard P, Buisson F, Lassalle-Balier G, Ledu M, Elisabether C, Passot X, Rey E (2006) The DEMETER microsatellite and ground segment. *Planet Space Sci* 54(5):413–427
- England SL, Maus S, Immel TJ, Mende SB (2006) Longitudinal variation of the E-region electric fields caused by atmospheric tides. *Geophys Res Lett* 33:L21105. <https://doi.org/10.1029/2006GL027465>
- England SL, Immel TJ, Huba JD, Hagan ME, Maute A, DeMajistre R (2010) Modeling of multiple effects of atmospheric tides on the ionosphere: an examination of possible coupling mechanisms responsible for the longitudinal structure of the equatorial ionosphere. *J Geophys Res* 115:A05308. <https://doi.org/10.1029/2009JA014894>
- Fejer BG, Jensen JW, Su SY (2008) Quiet time equatorial F region vertical plasma drift model derived from ROCSAT-1 observations. *J Geophys Res* 113:A05304. <https://doi.org/10.1029/2007JA012801>
- Forbes JM, Zhang X, Palo S, Russell J, Mertens CJ, Mlynczak M (2008) Tidal variability in the ionospheric dynamo region. *J Geophys Res* 113:e02310. <https://doi.org/10.1029/2007JA012737>
- Hagan ME, Maute A, Roble RG, Richmond AD, Immel TJ, England SL (2007) Connections between deep tropical clouds and the Earth's ionosphere. *Geophys Res Lett* 34:L20109. <https://doi.org/10.1029/2007GL030142>
- Hartman WA, Heelis RA (2007) Longitudinal variations in the equatorial vertical drift in the topside ionosphere. *J Geophys Res Space Phys* 112:A03305. <https://doi.org/10.1029/2006JA011773>
- Häusler K, Lühr H (2009) Nonmigrating tidal signals in the upper thermospheric zonal wind at equatorial latitudes as observed by CHAMP. *Ann Geophys* 27:2643–2652. <https://doi.org/10.5194/angeo-27-2643-2009>
- Henderson SB, Swenson CM, Christensen AB, Paxton LJ (2005) Morphology of the equatorial anomaly and equatorial plasma bubbles using image subspace analysis of Global Ultraviolet Imager data. *J Geophys Res* 110:A11306. <https://doi.org/10.1029/2005JA011080>
- Immel TJ, Sagawa E, England SL, Henderson SB, Hagan ME, Mende SB, Frey HU, Swenson CM, Paxton LJ (2006) Control of equatorial ionospheric morphology by atmospheric tides. *Geophys Res Lett* 33:L15108. <https://doi.org/10.1029/2006GL026161>
- Kakinami Y, Lin CH, Liu JY, Kamogawa M, Watanabe S, Parrot M (2011) Daytime longitudinal structures of electron density and temperature in the topside ionosphere observed by the Hinotori and DEMETER satellites. *J Geophys Res Space Phys* 116:A05316. <https://doi.org/10.1029/2010JA015632>
- Kelly MC (2009) *The Earth's ionosphere: plasma physics and electrodynamics*. Academic Press, MA, USA, p 73
- Kil H, Oh S-J, Kelley MC, Paxton LJ, England SL, Talaat E, Min K-W, Su S-Y (2007) Longitudinal structure of the vertical E × B drift and ion density seen from ROCSAT-1. *Geophys Res Lett* 34:L14110. <https://doi.org/10.1029/2007GL030018>
- Kil H, Talaat ER, Oh S-J, Paxton LJ, England SL, Su S-Y (2008) Wave structures of the plasma density and vertical E × B drift in low-latitude F region. *J Geophys Res* 113:A09312. <https://doi.org/10.1029/2008JA013106>
- Klotz S, Johnson NL (eds) (1983) *Encyclopedia of statistical sciences*. John Wiley, Hoboken
- Lin CH, Hsiao CC, Liu JY, Liu CH (2007) Longitudinal structure of the equatorial ionosphere: time evolution of the four-peaked EIA structure. *J Geophys Res* 112:A12305. <https://doi.org/10.1029/2007JA012455>
- Liu H, Yamamoto M, Lühr H (2009) Wave-4 pattern of the equatorial mass density anomaly: a thermospheric signature of tropical deep convection. *Geophys Res Lett* 36:L18104. <https://doi.org/10.1029/2009GL039865>
- Liu J-Y, Kan KW, Chao CK et al (2023) Nighttime wavenumber-four and plasma depletion bays observed by FORMOSAT-5/AIP, ICON/IVM, and COSMIC-2/RO data. *Adv Space Res*. <https://doi.org/10.1016/j.asr.2023.04.047>
- Oberheide J, Forbes JM, Häusler K, Wu Q, Bruinsma SL (2009) Tropospheric tides from 80 to 400 km: propagation, interannual variability, and solar cycle effects. *J Geophys Res* 114:D00105. <https://doi.org/10.1029/2009JD012388>
- Onohara AN, Batista IS, Batista PP (2018) Wavenumber-4 structures observed in the low-latitude ionosphere during low and high solar activity periods using FORMOSAT/COSMIC observations. *Ann Geophys* 36:459–471. <https://doi.org/10.5194/angeo-36-459-2018>
- Pedatella NM, Forbes JM, Oberheide J (2008) Intra-annual variability of the low-latitude ionosphere due to nonmigrating tides. *Geophys Res Lett* 35:L18104. <https://doi.org/10.1029/2008GL035332>
- Ren Z, Wan W, Liu L, Zhao B, Wei Y, Yue X, Heelis RA (2008) Longitudinal variations of electron temperature and total ion density in the sunset equatorial topside ionosphere. *Geophys Res Lett* 35:L05108. <https://doi.org/10.1029/2007GL032998>
- Sagawa E, Immel TJ, Frey HU, Mende SB (2005) Longitudinal structure of the equatorial anomaly in the nighttime ionosphere observed by IMAGE/FUV. *J Geophys Res* 110:A11302. <https://doi.org/10.1029/2004JA010848>
- Su S-Y, Yeh HC, Heelis RA, Wu JM, Yang SC, Lee LF, Chen HL (1999) The ROCSAT-1 IPEI preliminary results: low latitude ionospheric plasma and flow variations. *Terrestrial, Atmos Oceanic Sci* 10:787–804
- Wan W, Liu L, Pi X, Zhang M-L, Ning B, Xiong J, Ding F (2008) Wavenumber-4 patterns of the total electron content over the low latitude ionosphere. *Geophys Res Lett* 35:L12104. <https://doi.org/10.1029/2008GL033755>
- Wan W, Xiong J, Ren Z, Liu L, Zhang M-L, Ding F, Ning B, Zhao B, Yue X (2010) Correlation between the ionospheric WN4 signature and the upper atmospheric DE3 tide. *J Geophys Res* 115:A11303. <https://doi.org/10.1029/2010JA015527>
- Yeh HC, Su S-Y, Heelis RA, Wu JM (1999) The ROCSAT-1 IPEI preliminary results: vertical ion drift statistics. *Terrestrial, Atmos Oceanic Sci* 10:805–820

Publisher's Note

Springer Nature remains neutral with regard to jurisdictional claims in published maps and institutional affiliations.